Inorg. Chem. **2002**, *41*, 4018–4024

Mechanistic Studies of a Calcium-Dependent MRI Contrast Agent

Wen-hong Li,[||,†] Giacomo Parigi,[‡] Marco Fragai,[§] Claudio Luchinat,[‡] and Thomas J. Meade*[||,⊥]

Division of Biology and the Beckman Institute, California Institute of Technology, Pasadena, California 91125, and CERM and the Departments of Agricultural Biotechnology and Chemistry, University of Florence, Florence, Italy

Received January 14, 2002

Intracellular Ca^{2+} plays an important role in signal transduction, and we are developing new MRI techniques to study its regulation in living animals. We have reported on an MRI contrast agent (DOPTA-Gd) where the relaxivity of the complex is controlled by the presence or absence of the divalent ion Ca^{2+}. By structurally modulating inner-sphere access of water to a chelated Gd^{3+} ion, we observe a substantial and reversible change in T_1 upon the addition of Ca^{2+} and not other divalent ions. Luminescence lifetime and NMRD measurements of the complex have been acquired, and several parameters contribute to the Ca^{2+} dependent relaxivity change of DOPTA-Gd. The number of inner-sphere water molecules is more than doubled after the Ca^{2+} concentration is increased. This finding strongly supports the proposed conformational change of DOPTA-Gd when Ca^{2+} is bound. Relaxometric measurements confirm these results and provide an indication that second-sphere water molecules are probably responsible for paramagnetic relaxation enhancement in the absence of Ca^{2+}. After Ca^{2+} is bound to DOPTA-Gd, the molecule undergoes a substantial conformational change that opens up the hydrophilic face of the tetraazacyclododecane macrocycle. This change dramatically increases the accessibility of chelated Gd^{3+} ion to bulk solvent. The design of this class of calcium-activated MR contrast agent was based primarily on the assumption that the number of coordinated inner-sphere water molecules would be the dominating factor in observed relaxivity measurements. This result has been confirmed; however, careful mechanistic studies reveal that additional factors are involved in this process.

Introduction

The advent of microscopic magnetic resonance imaging (MRI) techniques for investigating biological processes, and the continued need for improvement in clinical MRI contrast agents, has stimulated a resurgence in MRI contrast agent research.[1] Recently, some of us reported on a novel class of biochemically triggered MR contrast agents for T_1-weighed imaging applications.[2−4] These agents are stable paramagnetic complexes containing Gd^{3+} ions that increase both the spin−lattice (T_1) and spin−spin (T_2) relaxation rates of water protons. Because the intrinsic T_2 relaxation rates of the fluid surrounding tissues and organs are fast, these agents are most effective in modulating T_1 and, therefore, the signal intensity of T_1-weighed images. Unlike MR contrast agents such as DOTA-Gd or DTPA-Gd that provide anatomical information,

* To whom correspondence should be addressed. E-mail: tmeade@caltech.edu.

† Current address: Department of Cell Biology, University of Texas Southwestern Medical Center, 5323 Harry Hines Blvd., Dallas, TX 75390-9039.

‡ CERM and the Department of Agricultural Biotechnology, University of Florence.

§ CERM and the Department of Chemistry, University of Florence.

|| California Institute of Technology.

⊥ Current address: Northwestern University, Department of Chemistry, Department of Biochemistry, Molecular Biology and Cell Biology, and Department of Physiology and Neurobiology, Evanston, IL 60208.

(1) (a) Mikawa, M.; Kato, H.; Okumura, M.; Narazaki, M.; Kanazawa, Y.; Miwa, N.; Shinohara, H. *Bioconjugate Chem.* **2001**, *12*, 510−514. (b) Bianchi, A. C. L.; Corana, F.; Fontana, S.; Losi, P.; Maiocchi, A.; Paleari, L.; Valtancoli, B. *Coord. Chem. Rev.* **2000**, *204*, 309−393. (c) Louie, A. Y.; Meade, T. J. *New Technol. Life Sci. Trends Guide* **2000**, December, 7−11. (d) Zhang, S.; Wu, K.; Sherry, A. *Angew. Chem., Int. Ed.* **1999**, *38*, 3192−3194. (e) Caravan, P.; Ellison, J.; McMurry, T.; Lauffer, R. *Chem. Rev.* **1999**, *99*, 2293−2352. (f) Reichert, D. E.; Lewis, J. S.; Anderson, C. J. *Coord. Chem. Rev.* **1999**, *184*, 3−66. (g) DeNardo, G. L.; Kroger, L. A.; Meares, C. F.; Richman, C. M.; Salako, Q.; Shen, S.; LAmborn, K. R.; Peterson, J. J.; Miers, L. A.; Zhong, G. R.; DeNardo, S. J. *Clin. Cancer Res.* **1998**, *4*, 2483−2490. (h) Aime, S.; Botta, M.; Fasano, M.; Terreno, E. *Chem. Soc. Rev.* **1998**, *27*, 19−29. (i) Tweedle, M. *Eur. Radiol.* **1997**, *7*, S225−S230. (j) Kayyem, J. F.; Kumar, R. M.; Fraser, S. E.; Meade, T. J. *Chem. Biol.* **1995**, *2*, 615−620.

(2) Moats, R. A.; Fraser, S. E.; Meade, T. J. *Angew. Chem., Int. Ed. Engl.* **1997**, 726−728.

(3) Li, W.; Fraser, S.; Meade, T. *J. Am. Chem. Soc.* **1999**, *121*, 1413−1414.

10.1021/ic0200390 CCC: $22.00
Published on Web 06/28/2002

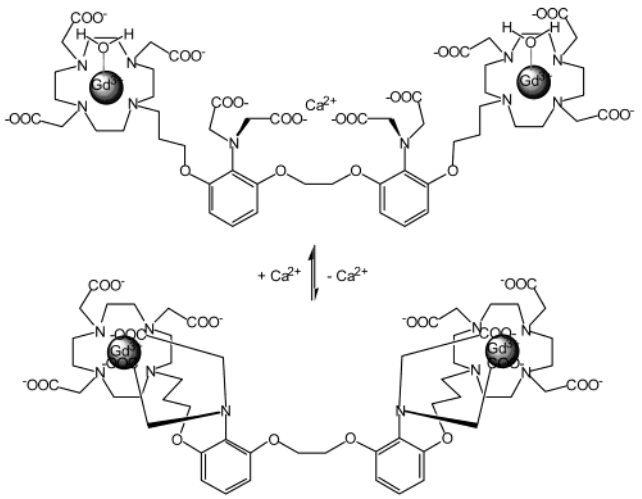

Figure 1. Proposed conformational change of a Ca^{2+} activated MR contrast agent.

these biologically activated MR contrast agents were designed as reporters to track biochemical changes of the local environment.

The relaxivity of these contrast agents is modulated by a specific biochemical trigger that can be enzymatic, or the binding of an intracellular messenger. To permit an in vivo assay of enzymatic activities, a contrast agent was synthesized with cleavable protection groups that largely prevent access of water to the paramagnetic center of the contrast agent. By limiting access of water to the lanthanide ion, the unprocessed agent is an ineffective contrast agent and, hence, serves as a reliable marker for regions of enzyme activity.

As a result, T_1-weighed MR images acquired in the presence of these agents detect the corresponding dynamics of internal physiology or biochemistry. An enzyme cleavable MRI contrast agent (Egad-Me) has been applied successfully in vivo to delineate patterns of gene expression in developing *Xenopus* embryos.[4] At cellular resolution, regions of higher intensity in the MR image correlated well with regions expressing marker enzyme. Combined with the power of MRI microscopy, this novel class of agents offers the promise of providing information on the internal physiology of living organisms at cellular resolution in the form of 3-D images in real time.[5]

Intracellular Ca^{2+} plays an important role in signal transduction, and we are interested in developing new MRI techniques to study its regulation in living animals. We recently reported the design and synthesis of a reversible calcium sensitive MRI contrast agent, DOPTA-Gd.[3] This macrocyclic dimer was synthesized from nitroresorcinol in 8 steps (including the addition of the Gd^{3+}) and displays a large and reliable relaxivity change in response to a physiological range of calcium concentration changes. The design of this contrast agent was based on the mechanism of inner-sphere relaxation coupled with a Ca^{2+}-dependent conformational switch (Figure 1). Specifically, the accessibility of water molecules to the bound Gd^{3+} ions and, hence, the relaxivity of DOPTA-Gd are controlled by Ca^{2+} concentration.

A number of parameters including the inner-sphere water exchange rate, rotational and electron spin correlation times, and the distance from the lanthanide ion to coordinated water protons contribute to the observed relaxivity value. Contributions by water protons from the first and second coordination spheres[23,24] and by outer-sphere[7] water protons may arise. To investigate the correlation of these parameters with varying Ca^{2+} concentration and the MR agent, we report luminescence lifetime and nuclear magnetic resonance relaxation dispersion (NMRD) measurements. NMRD profiles were fitted to the newly modified Solomon−Bloembergen−Morgan theory.[6,9,20−22,26] These data suggest that inner-sphere water molecules (both in the first and in the

(4) Louie, A. Y.; Hüber, M. M.; Ahrens, E. T.; Röthbacher, U.; Moats, R.; Jacobs, R.; Fraser, S. E.; Meade, T. J. *Nature Biotechnol.* **2000**, *18*, 321−325.
(5) Jacobs, R.; Ahrens, E.; Meade, T.; Fraser, S. *Trends Cell Biol.* **1999**, *9*, 73−76.
(6) (a) Bloembergen, N. *J. Chem. Phys.* **1957**, *27*, 572−573. (b) Solomon, I. *Phys. Rev.* **1955**, 559−565.
(7) (a) Bertini, I.; Luchinat, C.; Parigi, G. *Solution NMR of Paramagnetic molecules*; Elsevier: Amsterdam, 2001. (b) Hwang, L. P.; Freed, J. H. *J. Chem. Phys.* **1975**, *63*, 4017. (c) Polnaszek, C. F.; Bryant, R. G. *J. Chem. Phys.* **1978**, *68*, 4034.
(8) Luchinat, C.; Xia, Z. *Coord. Chem. Rev.* **1992**, *120*, 281−307.
(9) Bertini, I.; Galas, O.; Luchinat, C.; Parigi, G. *J. Magn. Reson., Ser. A* **1995**, *113*, 151−158.
(10) Horrocks, W. D., Jr.; Sudnick, D. R. *Acc. Chem. Res.* **1981**, *14*, 384−392. The quenching effect on the metal luminescence from bound water molecules arises from the vibronic coupling of O−H oscillators to the excited states of metals. The efficiency of such quenching is determined by two factors: the number of inner-sphere water molecules and the distance of inner-sphere water molecules to the metal center. For the same number of inner-sphere water molecules, they may quench the luminescence to different extents depending on how close they are to the metal. Thus, the *q* value obtained from luminescence lifetime measurements may actually reflect overall effects of two factors: number of water molecules and distance to the metal center. The appearance of fractional numbers is thus not unexpected. Unfortunately, we are unable to determine the relative contributions of these two factors from the luminescence measurements. Table 2 fixes the distance, *r*, at 3.1 Å for DOPTA-Gd and DOPTA-Gd-Ca, and allows other parameters to relax within a range and may need validation from experiments such as X-ray crystallographic analysis. Moreover, this equation was empirically derived from a limited number of lanthanide complexes, and the equation has an intrinsic uncertainty of 0.5 even for the group of complexes examined by them.
(11) Frey, S. T.; Chang, C. A.; Carvalho, J. F.; Varadarajan, A.; Schultze, L. M.; Pounds, K. L.; Horrocks, W. D. *Inorg. Chem.* **1994**, *33*, 2882−2889.
(12) Hemmila, I.; Mukkala, V. M.; Takalo, H. *J. Alloys Compd.* **1997**, *249*, 158−162.
(13) Richardson, F. S. *Chem. Rev.* **1982**, *82*, 541−552.
(14) Koenig, S. H.; Brown, R. D. *Magn. Reson. Med.* **1984**, *1*, 478−495.
(15) Muller, R. N.; Vander Elst, L.; Rinck, P. A.; Vallet, P.; Maton, F.; Fischer, H.; Roch, A.; Van Haverbeke, Y. *Invest. Radiol.* **1988**, *23*, S229−S231.
(16) Koenig, S. H.; Brown, R. D., III. *Prog. Nucl. Magn. Reson. Spectrosc.* **1990**, *22*, 487.
(17) Uggeri, F.; Aime, S.; Anelli, P. L.; Botta, M.; Brocchetta, M.; De Haen, C.; Ermondi, G.; Grandi, M.; Paoli, P. *Inorg. Chem.* **1995**, *34*, 633.
(18) Toth, E.; Connac, F.; Helm, L.; Adzamli, K.; Merbach, A. *Eur. J. Inorg. Chem.* **1998**, 2017.
(19) Aime, S.; Botta, M.; Geninatti Crich, S.; Giovenzana, G.; Pagliarin, R.; Sisti, M.; Terreno, E. *Magn. Reson. Chem.* **1998**, *36*, S200.
(20) Bloembergen, N.; Morgan, L. O. *J. Chem. Phys* **1961**, *34*, 842−850.
(21) Bertini, I.; Kowalewski, J.; Luchinat, C.; Nilsson, T.; Parigi, G. *J. Chem. Phys.* **1999**, *111*, 5795.
(22) Nilsson, T.; Kowalewski, J. *Mol. Phys.* **2000**, *98*, 1617.
(23) Chen, J. W.; Belford, R. L.; Clarkson, R. B. *J. Phys. Chem. A* **1998**, *102*, 2117.
(24) Botta, M. *Eur. J. Inorg. Chem.* **2000**, 399.

second coordination sphere) and other factors contribute to the observed Ca^{2+}-dependent relaxation processes. Further, we have measured the magnetic properties of DOPTA-Gd at low to medium field strengths used in clinical imaging.

Materials and Methods

Materials. $TbCl_3 \cdot 6H_2O$ (99.9%) and $GdCl_3 \cdot 6H_2O$ (99.9%) were purchased from Aldrich. Ethylene glycol bis(β-aminoethyl ether)-*N*,*N*,*N*′,*N*′-tetraacetic acid (EGTA, puriss, ≥99%), KCl (puriss, ≥99.5%), and $CaCl_2 \cdot 2H_2O$ (puriss, ≥99%) were purchased from Fluka. MOPS (3-[*N*-morpholino]propanesulfonic acid, ≥99.5) was purchased from Sigma. Deuterated glycerol (1,1,2,3,3-D5, 99%) was purchased from Cambridge Isotope Laboratory (Andover, MA). Chelex 100 resin was obtained from Bio-Rad Laboratories (Hercules, CA). Unit mass determinations were carried out at the Caltech Protein Microanalytical Laboratory using a Perkin-Elmer/Sciex API 365 triple quadrupole mass spectrometer operated in the electrospray ionization mode. The Gd^{3+} content of samples was determined by an inductively coupled plasma mass spectrometer (ICP-MS, Perkin-Elmer/Sciex Elan 5000A) at the Bank of America Environmental Analysis Center at Caltech. The luminescence spectra of DOPTA-Tb were recorded on a Hitachi F-4500 fluorometer. Tb^{3+} luminescence lifetime measurements were acquired in the slow phosphorescence lifetime mode.

Synthesis of Lanthanide Complexes of DOPTA. The free ligand DOPTA was synthesized from 2-nitroresorcinol in 7 steps as described.[3] Insertion of Tb^{3+} ions into the macrocyclic dimer was carried out in a weakly acidic aqueous solution. Briefly, DOPTA (20 mg, 14.2 mmol) was dissolved in 2 mL of distilled water. $TbCl_3 \cdot 6H_2O$ (11.6 mg, 31 mmol) was added. The solution was stirred at room temperature for 24 h during which aliquots of NaOH were added to maintain the pH around 6.5. The reaction mixture was passed through an ion exchange column packed with Chelex 100 resin. Eluants containing the product were collected and further purified by reverse phase chromatography (Lichroprep RP-18, EM Separations). The final product appeared as a white powder after freeze-drying. Mass spectroscopy showed several major peaks corresponding to different ionization adducts of DOPTA-Tb. These peaks include 1591.2 (1591.37 calcd for $[C_{56}H_{78}N_{10}O_{24}Tb_2 - H^+]^-$), 795.0 (795.2 calcd for $[M - 2H^+]^{2-}$), 1613.2 (1613.35 calcd for $[M + Na^+ - 2H^+]^-$), and 1635.4 (1635.33 calcd for $[M + 2Na^+ - 3H^+]^-$).

DOPTA-Gd was prepared in a similar fashion as DOPTA-Tb. Mass spectroscopy revealed multiple peaks with the characteristic isotope distribution of Gd^{3+} ion. Major peaks observed for $[C_{56}H_{78}N_{10}O_{24}Gd_2{}^+Na^+ - 2H^+]^-$ include 1605.2, 1606.4, 1607.2, 1608.4, 1609.4, 1610.4, 1611.4, 1612.2, 1613.4, 1614.4, and 1615.2, with the peak at 1611.4 of the highest intensity. The peak distribution is in excellent agreement with the mass spectrum predicted by the Isotope Pattern Calculator (THINK Technologies Inc.).

Luminescence Lifetime Measurements of DOPTA-Tb. All measurements were carried out in solutions containing 100 μM DOPTA-Tb, 100 mM KCl, and 10 mM KMOPS. The Ca^{2+}-free buffer contained 1mM EGTA, and the high Ca^{2+} buffer contained 1mM CaEGTA and 1mM $CaCl_2$. The final pH of all solutions was adjusted with KOH or HCl to 7.20. The luminescence decay was recorded in the short phosphorescence lifetime mode and was repeated at least 20 times under each condition. The luminescence lifetime was calculated from the monoexponential fitting of the average decaying data.

Nuclear Magnetic Resonance Dispersion Measurements of DOPTA-Gd. The stock solution of DOPTA-Gd in 10 mM KMOPS buffer (pH 7.20) was diluted with buffers containing either 10 mM KMOPS, 100 mM KCl, 10 mM EGTA, pH 7.20 (0 Ca^{2+}), or 10 mM KMOPS, 100 mM KCl, 10 mM EGTA-Ca, 10 mM $CaCl_2$, pH 7.20 (high Ca^{2+}). Glycerol solutions were prepared by mixing the buffers with 1,1,2,3,3-deuterated glycerol (60 wt %). The final concentration of contrast agents is determined by measuring the Gd^{3+} content by ICP-MS.

Longitudinal water proton relaxation rates were measured with a Stelar prototype fast field cycling relaxometer (0.01−15 MHz proton Larmor frequency range) and with a Bruker CXP90 spectrometer (15−80 MHz proton Larmor frequency range).[7,8] These instruments provide R_1 values with an error of approximately 1%. Proton nuclear magnetic relaxation dispersion (NMRD) profiles have thus been obtained by plotting proton relaxation rates as a function of applied magnetic field. NMRD data, subtracted from the diamagnetic contribution of buffers alone, were analyzed in terms of inner-sphere and outer-sphere effects according to existing theories.[7,9]

Theoretical Background. The enhancement of the relaxation rates in the presence of paramagnetic species results from both inner-sphere and outer-sphere contributions. The outer-sphere contribution is due to water diffusion from infinity to the distance of closest approach, *d*, with a diffusional correlation time, τ_D.[7] The inner sphere longitudinal relaxation rate is given by

$$\frac{1}{T_1^{IS}} = \frac{qP_m}{T_{1M} + \tau_M} \tag{1}$$

where q is the number of inner-sphere water molecules, τ_M is the residence lifetime of water protons in the inner coordination sphere, and T_{1M} is the longitudinal relaxation time of coordinated water protons. qP_m is the mole fraction of water molecules bound to metal centers.

The paramagnetic dipole−dipole relaxation rate can be described by the Solomon−Bloembergen equation:[6,7]

$$\frac{1}{T_1^{dip}} = \frac{2}{15}\left(\frac{\mu_0}{4\pi}\right)^2 \frac{\gamma_N{}^2 g_e{}^2 \mu_B{}^2 S(S+1)}{r^6}\left[\frac{3\tau_c}{(1+\omega_I{}^2\tau_c{}^2)} + \frac{7\tau_c}{(1+\omega_s{}^2\tau_c{}^2)}\right] \tag{2}$$

where μ_0 is the permeability of vacuum, γ_N is the proton magnetogyric ratio, g_e is the electronic g factor, μ_B is the Bohr magneton, ω_I and ω_s are the Larmor procession frequencies for the nuclear and electron spins, and r is the metal electron spin-water proton distance. S is the total electron spin of the metal ion. The correlation time ,τ_c, modulating proton relaxation, is composed of contributions from rotational correlation time, τ_r, longitudinal electronic relaxation time, τ_s, and chemical exchange lifetime, τ_M, according to the equation:

$$\frac{1}{\tau_c} = \frac{1}{\tau_s} + \frac{1}{\tau_M} + \frac{1}{\tau_r} \tag{3}$$

The rotational correlation time can be estimated from the Stokes−Einstein equation:

$$\tau_r = \frac{4\pi a^3 \eta}{3kT} \tag{4}$$

(25) (a) Bligh, S. W. A.; Chowdhury, A. H. M. S.; Kennedy, D.; Luchinat, C.; Parigi, G. *Magn. Res. Med.* **1999**, *41*, 767. (b) Anelli, P. L.; Bertini, I.; Fragai, M.; Lattuada, L.; Luchinat, C.; Parigi, G. *Eur. J. Inorg. Chem.* **2000**, 625.
(26) Kowalewski, J.; Luchinat, C.; Nilsson, T.; Parigi, G. *Magn. Res. Med.*, submitted.

where a is the radius of the spherical-modeled molecule, η is the viscosity of the solvent, k is the Boltzmann constant, and T is the temperature.

The electronic relaxation time is generally dependent on the magnetic field strength. For Gd^{3+}, the magnitude of electronic relaxation rate is determined by the amplitude of the transient ZFS, caused by the collisions of water molecules, and by the electron correlation time, τ_v, according to the Bloembergen−Morgan equation:[20]

$$\tau_s^{-1} = \frac{\Delta_t^2(4S(S+1)-3)}{25}\left(\frac{\tau_v}{1+\omega_s^2\tau_v^2}+\frac{4\tau_v}{1+4\omega_s^2\tau_v^2}\right) \quad (5)$$

where ω_s is the electron Larmor frequency and Δ_t^2 is the average quadratic transient zero field splitting. From the previous equation, the limiting value of τ_s at zero field can be calculated to be

$$\tau_{s,0}^{-1} = (\Delta_t^2/5)\,[4S(S+1)-3]\tau_v \quad (6)$$

Increasing the electronic relaxation time results in a longer effective correlation time for the electron−nuclear interaction (if the rotational time is longer than τ_s) which in turn leads to a larger nuclear spin relaxation rate. Equation 5 has been derived in the absence of a static ZFS term in the electron Hamiltonian, and it provides an "average" electron relaxation time for the various nondegenerate transitions. Programs have been developed for a better estimation of the electron relaxation time, to take into account these further effects.[21,22]

Results and Discussion

Luminescence Spectra of DOPTA-Tb. A direct test of the proposed conformational change shown in Figure 1 would be to determine the number of water molecules in the first coordination sphere before and after Ca^{2+} is added. Measuring luminescence lifetimes of lanthanide complexes has been widely used for quantifying the number of inner-sphere water molecules.[10] Tb^{3+} and Eu^{3+} are commonly used for lifetime measurements because they emit in the visible region when their 4f electrons relax from higher energy levels to the lowest energy multiplets. We prepared the Tb^{3+} complex of DOPTA as a homologue of DOPTA-Gd. Because these two ions have nearly the same charge to ionic radius ratio and similar coordination chemistry, the number of inner-sphere water molecules estimated for Tb^{3+} complexes should be close to the value for the corresponding Gd^{3+} complexes.[11]

The excitation and emission spectra and the luminescence decay curve of DOPTA-Tb in Ca^{2+} free buffer are shown in Figure 2. A desirable optical property of DOPTA-Tb is that the aminobisphenoxy moiety can act as an antenna to sensitize the emission of Tb^{3+} as indicated by the absorption and excitation spectrum of DOPTA-Tb (data not shown). The aminobisphenoxy moiety absorbs strongly between 220 and 280 nm. After excitation, the chromophore transfers energy to the nearby Tb^{3+} ion which emits from the $^5D_4$ state to the ground-state manifolds (^7F_J, $J = 0-6$). Because of the intrinsic low absorbance of metal ions, organic chromophores that can sensitize the emission of Tb^{3+} and other lanthanide ions greatly increase the effective extinction coefficient of metal ion excitation and therefore improve the sensitivity of luminescence detection.[12]

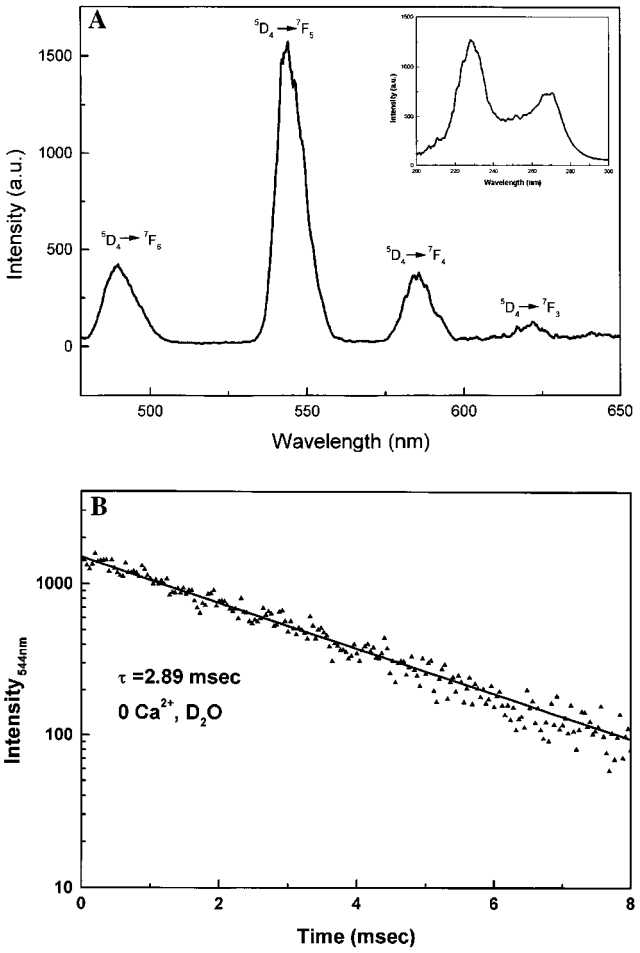

Figure 2. (A) Emission and excitation (insert) spectra of DOPTA-Tb. The emission spectrum was recorded at the excitation wavelength of 265 nm, and the excitation spectrum was measured by monitoring the emission at 545 nm. (B) Luminescence decay curve of DOPTA-Tb in Ca^{2+} free buffer. Excitation 265 nm; emission 545 nm.

The emission spectrum of DOPTA-Tb appears as sharp peaks because 4f orbitals of lanthanides are largely shielded from the environment and are minimally involved in bonding. The strongest emission peak centered at 544 nm corresponds to $^5D_4$ Π $^7F_5$ transition. The excitation and emission spectra of DOPTA-Tb in Ca^{2+} buffer are similar to those obtained in Ca^{2+} free buffer, with the emission peaks slightly broadened (especially 584 and 622 nm). In addition, the relative peak heights of Tb^{3+} emission changed after addition of Ca^{2+}. The relative intensities of the $^5D_4$ Π ^7F_J emission bands are sensitive to the nature of the ligand environment[13] and suggest changes in the coordination environment of DOPTA-Tb when Ca^{2+} concentration varies (vide infra).

The peak emission intensity of DOPTA-Tb at 544 nm in high Ca^{2+} buffer is less than half that in Ca^{2+} free buffer. This may be due to a reduced quantum yield of Tb^{3+} emission in high Ca^{2+} buffer resulting from increased nonradiative relaxation. The energy transfer efficiency from the sensitizer to Tb^{3+} ion may also change when the conformation of DOPTA-Tb changes with respect to the Ca^{2+} concentrations. However, when we compared the emission intensities of DOPTA-Tb in D_2O at 1 mM Ca^{2+} versus 0 Ca^{2+}, the difference in emission intensity is less than half

Table 1. Luminescence Lifetimes (Reciprocal) and the Number of Inner-Sphere Water Molecules of DOPTA-Tb in the Presence and Absence of Ca^{2+}

	τ_{H_2O} (ms)	τ_{D_2O} (ms)	τ_{H_2O}/τ_{D_2O}	q^a
0 Ca^{2+}	2.187 (0.457)	2.89 (0.346)	0.757	0.47 ± 0.5
1 mM Ca^{2+}	1.76 (0.568)	3.139 (0.318)	0.561	1.05 ± 0.5

[a] Calculated from Horrocks' equation (see text).

of the change measured in H_2O, suggesting that the nonradiative relaxation played a major role in quenching Tb^{3+} luminescence at high Ca^{2+} concentration. Because of the vibronic coupling of O−H oscillators to the $^5D_4$ emissive level of Tb^{3+}, the $^5D_4$ state of Tb^{3+} is relaxed nonradiatively by bound water molecules. This additional relaxation pathway results in the shortening of the luminescence lifetime of DOPTA-Tb when Ca^{2+} is bound. Replacing water with deuterium oxide greatly reduces the efficiency of vibronic coupling and leads to increased luminescence lifetime in D_2O. The difference of luminescence lifetimes in H_2O and D_2O directly reflects number of inner-sphere water molecules, q, and can be estimated by applying the equation developed by Horrocks et al.[10]

$$q = 4.2\left(\frac{1}{\tau_{H_2O}} - \frac{1}{\tau_{D_2O}}\right) \quad (7)$$

where τ is the luminescence lifetime of Tb^{3+} complexes in H_2O or D_2O.

Figure 2B shows a luminescence decay curve of DOPTA-Tb in Ca^{2+} free buffer in D_2O. Under all conditions, the emission of DOPTA-Tb strictly followed single-exponential decay as analyzed by the least-squares analysis. The luminescence lifetime and the number of water molecules in the first coordination sphere of DOPTA-Tb are summarized in Table 1. As shown in Figure 1, the proposed conformational dependence of DOPTA-Tb with respect to Ca^{2+} predicts that there should be more water molecules directly bound to the chelated lanthanide metal in the presence of Ca^{2+} than in the absence of Ca^{2+}. Indeed, the number of inner-sphere water molecules increases from 0.47 to 1.05 upon addition of Ca^{2+} as measured by luminescence lifetimes of Tb^{3+} complexes. This result provides the strongest support for the proposed conformational change of DOPTA complex with respect to Ca^{2+} concentration. This is consistent with the expected binding between Ca^{2+} ion and the two pairs of iminoacetates of the BAPTA moiety. In the absence of Ca^{2+}, one or more carboxylate groups are coordinated to lanthanide ions. After binding to Ca^{2+}, an open coordination site is available for a water molecule.

NMRD Measurements of DOPTA-Gd and Data Analysis. To investigate the mechanisms of calcium-dependent relaxivity change of DOPTA-Gd, we carried out nuclear magnetic relaxation dispersion (NMRD) measurements. NMRD measurements determine the field-dependent relaxivity changes of paramagnetic compounds using a field cycling relaxometer.[14] The resulting NMRD profiles may be analyzed according to Solomon−Bloembergen−Morgan theory to interrogate relative contributions of individual parameters to the overall relaxivity variation and may provide insight on mechanisms governing relaxation processes.[7,15] We limit our discussion to longitudinal (spin−lattice) relaxation because DOPTA-Gd was designed as a T_1 agent for MRI.

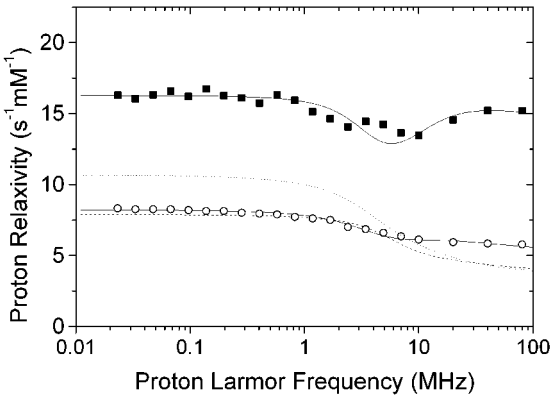

Figure 3. ^1H NMRD profiles of DOPTA-Gd (○) and DOPTA-Gd−Ca (■) solution at 298 K. The solid lines represent the best fit profiles of the two sets of data. Dotted and dashed lines report the relaxivity profile of DOTA-Gd and DTPA-Gd, respectively.

The NMRD data for DOPTA-Gd in the absence and presence of Ca^{2+} have been acquired at 298 K in water (Figure 3). The profiles have been normalized to 1 mM Gd^{3+} ion concentration and fitted according to the Solomon−Bloembergen−Morgan theory. Both the inner- and outer-sphere contributions were taken into consideration, and the best fit parameters were reported in Table 2. Two commonly used contrast agents, DOTA-Gd and DTPA-Gd, have also been listed together for comparisons. From here on, we use DOPTA-Gd-Ca^{2+} to refer to the Ca^{2+} bound state of DOPTA-Gd, and DOPTA-Gd to refer to the Ca^{2+} free state. In the fits, τ_M, τ_v, Δ_t, and q have been left free to change, while τ_r and the metal−proton distance r were fixed. In fact, the value of r is known to a very good approximation from many previous studies on similar Gd complexes.[16−19] From the Stokes equation, τ_r is expected to be three times longer for DOPTA-Gd than for DTPA-Gd, and thus, in aqueous solution at 298 K, it is expected to be about 220 ps. In any case, even if r and τ_r were somewhat different from the imposed values, what is important for our study is that their values do not change appreciably in the presence and in the absence of Ca^{2+}, which is a reasonable assumption. Data have been analyzed with a Monte Carlo method, by simulating 1000 sets of data for each profile and including a stochastic error with a Gaussian distribution (the variance was set equal to 0.5 and 1 s^{-1} for data relative to DOTA-Gd and DOTA-Gd-Ca^{2+}, respectively). The best fit values and the errors reported in Table 2 are the mean value and the standard deviation of the best fit values obtained for the 1000 different fits.

From the fit, it is clear that $\tau_M \gg \tau_c$. Indeed, it was expected that the chemical exchange lifetime is much longer than τ_r, being less than microsecond for DTPA-Gd[16−18] and DOTA-Gd.[16,19] Furthermore, additional measurements performed at 308 K (not reported) show the occurrence of a fast exchange regime ($\tau_M < T_{1M}$, see eq 1), as proton relaxation rate decreases with increasing temperature. This

Table 2. Best-Fit Values of the NMRD Data of DOPTA-Gd and DOPTA-Gd-Ca^{2+} in Aqueous Solutions to Solomon−Bloembergen−Morgan Equation[a]

	τ_r 10^{-12} s	τ_M (*) 10^{-6} s	τ_v (*) 10^{-12} s	Δ_t (*) cm^{-1}	q (*)	r Å	τ_{s0} 10^{-12} s
DTPA-Gd	58−73	0.3	18−25	0.034−0.037	1	3.1	82−95
DOTA-Gd	72	0.3	26	0.014	1	3.1	458
DOPTA-Gd	200	0.2 ± 0.1	32 ± 8	0.029 ± 0.007	0.7 ± 0.1	3.1	87
DOPTA-Gd-Ca	200	0.2 ± 0.1	33 ± 8	0.031 ± 0.003	2.3 ± 0.2	3.1	74
DOPTA-Gd	220	0.2 ± 0.1	35 ± 9	0.026 ± 0.006	0.6 ± 0.1	3.1	99
DOPTA-Gd-Ca	220	0.2 ± 0.1	36 ± 6	0.029 ± 0.003	2.1 ± 0.1	3.1	77
DOPTA-Gd	240	0.15 ± 0.1	38 ± 10	0.024 ± 0.005	0.5 ± 0.1	3.1	107
DOPTA-Gd-Ca	240	0.15 ± 0.1	40 ± 7	0.026 ± 0.003	1.9 ± 0.1	3.1	87

[a] In all fits, the distance of closest approach, d, was fixed at 3.6 Å. The diffusion constant was fixed at 2.6×10^{-5} cm^2 s^{-1}. Fitted parameters are labeled with (*).

is in agreement with the best fit value for τ_M shorter than 10^{-6} s. Therefore, a more accurate determination of the exchange time is not relevant for the present study, as a nonexact value of τ_M cannot affect the value of the other parameters sizably.

Calculations were also performed by fixing the value of τ_r to 200 and 240 ps, instead of 220 ps. Best fit values (see Table 2) show that indeed the value of q decreases with increasing τ_r for both DOPTA-Gd and DOPTA-Gd-Ca, thus leaving the resulting overall picture unchanged. In the worst case (e.g., τ_r equal to 200 ps for DOPTA-Gd and to 240 ps for DOPTA-Gd−Ca), still q is 0.7 versus 1.9; that is, the difference in the number of coordinated water molecules remains very large and much larger than the error.

Physical Insight. (a) Transient ZFS. In Figure 3, the NMRD profiles of DOPTA-Gd, DTPA-Gd, DOTA-Gd, and DOPTA-Gd-Ca^{2+} are reported. All profiles exhibit an inflection point from about 1 to about 10 MHz. This corresponds to the ω_S dispersion. It is well-known that, although relaxivities of DOTA-Gd and DTPA-Gd at high field (>10 MHz) are similar, DTPA-Gd becomes less efficient in shortening spin−lattice relaxation time at lower field. This has been attributed to the lower molecular symmetry of DTPA-Gd, which is probably related to an increased transient ZFS, Δ_t, whose fluctuations cause electron relaxation. The electronic relaxation time at low field, τ_{s0}, of DTPA-Gd is in fact about five times shorter than that of DOTA-Gd. The Δ_t and τ_{s0} values of DOPTA-Gd are much closer to those of DTPA-Gd than DOTA-Gd. This may reflect the fact that, because DOPTA-Gd has less symmetrical structure than DOTA-Gd, it may be subjected more to instantaneous distortions through solvent collisions and molecular vibrations which modulate the zero field splitting of the metal ion.

(b) Relevant Correlation Times. In the absence of Ca^{2+}, the relaxivity of DOPTA-Gd is higher than that of DOTA-Gd at high field but lower than that of DOTA-Gd at low field. The change in the order of relaxivity values of these two agents can be rationalized on the basis of relative contributions of τ_s, τ_r, and q to the relaxivity. In the low field limit, the relaxivity of DOPTA-Gd is mainly determined by τ_{s0} (because $\tau_{s0}^{-1} > \tau_r^{-1}$), and the relaxivity of DOTA-Gd is largely controlled by τ_r (because $\tau_r^{-1} > \tau_{s0}^{-1}$). The value of τ_{s0} of DOPTA-Gd and the value of τ_r of DOTA-Gd are comparable. However, because the q value of DOTA-Gd is about twice as much as that of DOPTA-Gd, the relaxivity of DOTA-Gd is higher. At the proton Larmor frequencies higher than 10 MHz, τ_s increases because of its field dependence (eq 5), and according to eq 3, τ_r can thus dominate in determining the value of τ_c. The three times larger value of τ_r in DOPTA-Gd with respect to DOTA-Gd causes the higher relaxivity values of the former complex at high fields.

(c) Hydration in the Absence and Presence of Ca^{2+}. One of the most remarkable findings from the fitting was that the number of water molecules coordinated to the metal center increases significantly when Ca^{2+} was added to a Ca^{2+} free buffer. After DOPTA-Gd binds to Ca^{2+} (and fixing a distance between water protons and paramagnetic center of 3.1 Å typical of such systems (Table 2)), this number increases from 0.6 to slightly more than 2. The findings indicate an increased accessibility of Gd^{3+} ions to inner-sphere water molecules. After aromatic aminoacetates bind to Ca^{2+}, the chelated Gd^{3+} is more open to bulk solvents, resulting in stronger interactions between Gd^{3+} and coordinated water molecules.

In the absence of calcium, one water molecule may be present at a distance of about 3.3−3.4 Å. This could indicate the presence of one water proton hydrogen bonded to a carboxylate of the macrocyle. Alternatively, two second-sphere water molecules could be coordinated at a distance of about 3.8 Å from the metal ion, or a larger number of water molecules at larger distance.[23]

NMRD Measurements of DOPTA-Gd under Slow Rotation Conditions. Table 2 shows that rotational time and electron relaxation time are of the same order of magnitude. Therefore, both of them contribute to the correlation time for nuclear relaxation (see eq 3). To better investigate electron relaxation, it is important that the latter coincides with τ_c. This is achieved by increasing the rotational time by adding glycerol, so that viscosity is increased (see eq 4). This also permits us to simulate the condition of slow molecular rotation that may arise in vivo in case the contrast agent binds to macromolecular systems. Relaxivity was thus measured in 60% glycerol solution (Figure 4). In the presence of 60% glycerol, the viscosity is increased by a factor of 10, and therefore, the rotational time is 10 times longer (eq 4). The effect of a small static zero field splitting (D) also needed to be introduced to better reproduce the profile, as required for many protein−Gd^{3+} complex adducts exhibiting slow rotational behavior.[25] A fit was thus performed with a program (NMRD) developed by some of us,[9] which includes

Table 3. Best-Fit Values, Obtained with the Modified NMRD Program, of the NMRD Data of DOPTA-Gd and DOPTA-Gd-Ca in 60% Glycerol Solution[a]

	$\tau_v\,10^{-12}$ s	Δ_t cm^{-1}	q	D (ZFS) cm^{-1}	$\tau_{S0}\,10^{-12}$ s
DOPTA-Gd	25 ± 5	0.013 ± 0.001	0.76 ± 0.03	0.04 ± 0.01	555
DOPTA-Gd-Ca	22 ± 5	0.014 ± 0.001	1.41 ± 0.06	0.04 ± 0.01	544

[a] In all fits, the distance of closest approach, d, was fixed at 3.6 Å, the diffusion constant at 0.6×10^{-5} cm^2 s^{-1}, τ_M at 1.0×10^{-7} s, τ_r at 2×10^{-9} s, and r at 3.1 Å.

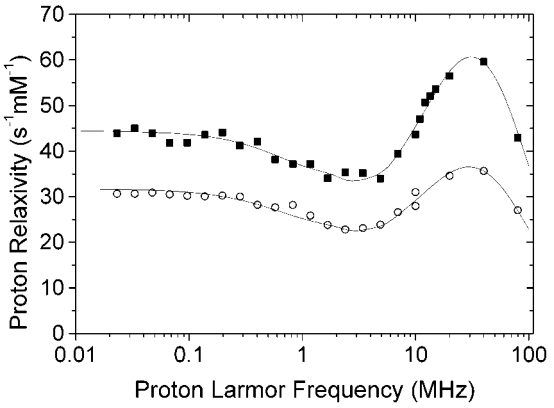

Figure 4. ^{1}H NMRD profiles of DOPTA-Gd (○) and DOPTA-Gd-Ca (■) in water solution with 60% glycerol at 298 K. The solid lines represent the best fit profiles of the two sets of data.

the presence of static ZFS and electron relaxation rates calculated according to eq 5. A modified version of such a program was recently developed in order to take into account the simultaneous presence of static and transient ZFS.[22,26] We also used this modified version of the program to fit the profiles, and this is the first time it has been used to fit experimental NMRD profiles of Gd(III) complexes. The best fit parameters are reported in Table 3. The best fit values of D and τ_v results are somewhat larger with the modified NMRD program, all other parameters (including q) being practically unchanged. Some uncertainty in the value of fitting parameters may be introduced by the value of the angle defining the position of the water proton(s) in the molecular frame, and by the value of the diffusion constant, which decreases as viscosity increases, although by a smaller extent as the diffusion constant depends on the microscopic viscosity.

The introduction of glycerol increased the values of relaxivity and modified the shape of the dispersion curve. The profile exhibits three inflections. The first one centered at about 1 MHz is attributed to the ω_s dispersion. The following peak relaxivity centered at about 30 MHz is the result of the field-dependent electron relaxation, and the last inflection, for frequency higher than 30 MHz, is related to the ω_I dispersion. This behavior results from a change in the correlation time τ_c which becomes highly sensitive to the electron relaxation field dependence when the rotational time is largely increased. The decay of the electron relaxation rate as a function of the magnetic field and the large value of the rotational time are in fact responsible for the peak relaxivity in the 10−50 MHz region of the proton relaxation rate. These measurements pointed to the important interplay between the electron spin-relaxation contribution to the correlation time for the electron−nuclear coupling and rotational correlation time of metal complexes. Again, the number of coordinated water molecules increases (from 0.7 to 1.4) after binding of Ca^{2+}. In the presence of Ca^{2+}, a value of q smaller than what was obtained in pure water solution is consistent with the possibility that glycerol may replace water in the coordination site.

Conclusions

In summary, by using a combination of techniques including luminescence lifetime and NMRD measurements, we have demonstrated that several parameters contribute to the Ca^{2+} dependent relaxivity change of DOPTA-Gd. From the luminescence lifetime measurements, we showed that the number of inner-sphere water molecules is more than doubled after the Ca^{2+} concentration is increased to a high level. This finding strongly supports the proposed conformational switch of DOPTA-Gd when Ca^{2+} is bound. Relaxometric measurements confirm this result and provide an indication that second-sphere water molecules are probably responsible for paramagnetic relaxation enhancement in the absence of Ca^{2+}. After Ca^{2+} is bound to DOPTA-Gd, the molecule undergoes a substantial conformational change that opens up the hydrophilic face of tetraazacyclododecane macrocycle. This change dramatically increases the accessibility of chelated Gd^{3+} ion to bulk solvent.

Acknowledgment. The work was supported by the Biological Imaging Center of the Beckman Institute, National Institutes of Health, the Human Brain Project, and CNR, Italy, Contracts 970113349 and 01.00832.PF28. W.-h.L. was supported by a fellowship from the American Heart Association, Western States Affiliates. We thank Drs. Gary M. Hathaway and Jie Zhou at the Caltech Protein Microanalytical Laboratory for performing mass spectroscopy analysis.

IC0200390